Advanced Composite Materials
Publication details, including instructions for authors and subscription information:
http://www.tandfonline.com/loi/tacm20

Micro-indentation method for evaluation of fracture toughness and thermal residual stresses of SiC coating on carbon/carbon composite

Hiroshi Hatta , Masayuki Mizoguchi , Masashi Koyama , Yuko Furukawa & Toshio Sugibayashi

Version of record first published: 02 Apr 2012.

To cite this article: Hiroshi Hatta , Masayuki Mizoguchi , Masashi Koyama , Yuko Furukawa & Toshio Sugibayashi (2003): Micro-indentation method for evaluation of fracture toughness and thermal residual stresses of SiC coating on carbon/carbon composite , Advanced Composite Materials, 12:2-3, 155-169

To link to this article: http://dx.doi.org/10.1163/156855103772658533

Adv. Composite Mater., Vol. 12, No. 2-3, pp. 155–169 (2003)

Also available online - www.vsppub.com

Micro-indentation method for evaluation of fracture toughness and thermal residual stresses of SiC coating on carbon/carbon composite

HIROSHI HATTA [1,*], MASAYUKI MIZOGUCHI [2], MASASHI KOYAMA [3], YUKO FURUKAWA [3] and TOSHIO SUGIBAYASHI [2]

[1] *Research Division of Space Propulsion Institute of Space and Astronautical Science, 3-1-1, Yoshinodai, Sagamihara, Kanagawa 229-8510, Japan*
[2] *Department of Mechanical Engineering, Takushoku University, 815-1 Tate-machi, Hachioji 193-0985, Japan*
[3] *Department of Material Science and Technology, Tokyo University of Science, 2641, Yamazaki, Noda-shi, Chiba-ken 278-8510, Japan*

Received 25 June 2002; accepted 24 January 2003

Abstract—Carbon/carbon composites are frequently used with SiC coating so as to improve their oxidation resistance. This oxidation protection coating has a thickness of about 100 μm, so that the properties of the coating might be different from those of bulk materials. However, it is rather difficult to determine mechanical properties of coatings by the usual procedures. In the present paper, a micro-indentation method was adopted to determine the fracture toughness and thermal residual stresses of SiC coatings. It was concluded that fracture toughness can be evaluated if the indentation load is sufficiently low, and thermal residual stress can be roughly determined, though scattering of the latter was large.

Keywords: SiC coating; fracture toughness; micro-indentation; C/C composite; thermal stress.

1. INTRODUCTION

Carbon fiber-reinforced carbon matrix composites (C/Cs) are expected to be applied to structures used at temperatures exceeding 1800 K, because they are the only material known to maintain high strength and toughness in such environments [1–4]. However, C/Cs are still at an early stage of development, and more experimentation must be done before C/Cs are applied to primary load bearing structures. The most serious problem with C/Cs is that they are vulnerable to oxygen attack at elevated temperatures [5–8]. To improve their oxidation

*To whom correspondence should be addressed. E-mail: hatta@pub.isas.ac.jp

resistance, various coatings to be applied to the surface of C/Cs have been investigated [1, 7–10]. Silicon carbide (SiC) coating, due to its stability at elevated temperatures and relatively low thermal expansion, has been most widely examined. However, excellent coating on a C/C is not easily formed. The thermal barrier coatings are usually applied at temperatures exceeding 1200 K, and the coefficient of thermal expansion (CTE) of a substrate C/C is, in general, extremely low. Accordingly, during the process of cooling from the coating forming temperature, cracking and/or debonding of the coating are usually induced. To protect against oxygen ingression through these defects, a glass sealant is over-coated on the thermal barrier coating. However, no sealant effective at temperatures exceeding 1200 K has yet been found. This indicates that, under current technology, C/Cs cannot be used stably for long time under oxidative and high temperature environments. Thus, to improve the performance of thermal barrier coatings on C/C substrates, an understanding of thermal stresses induced in the coating process and the corresponding mechanical properties of the coating is required.

In the present paper, we report an attempt to evaluate the fracture toughness of SiC coating formed on a substrate C/C and the thermal residual stress induced in the coating process. The thermal barrier coating usually has a thickness with an order of magnitude of 100 μm. Thus, the properties should be different from those of bulk material. Due to the thickness of the coating, it is not easy to measure its mechanical properties; reported results are scarce [11, 12]. The indentation method using a micro-hardness tester [13, 14] was adopted in the present study to determine the fracture toughness of the SiC coating and the thermal residual stress in the coating.

2. EXPERIMENTAL

2.1. Materials

Two unidirectionally reinforced C/Cs fabricated by the preformed yarn method [15] were used as substrates for SiC coating. Different suppliers made these C/Cs. Across Co., Japan, fabricated an Acro-C/C plate 3-mm thick; Advanced Materials Co., Japan, supplied an Adva-C/C plate 10-mm thick. The Acro-C/C was primarily used for the measurements of fracture toughness and thermal stress, and the Adva-C/C was used for supplemental purposes. The nominal fiber volume fraction of both C/Cs was 50%.

A silicone carbide coating was formed on the surfaces of the C/Cs by a chemical vapor deposition (CVD) method at 1473 K. Underneath the coating, a conversion layer of several μm thickness was formed by a chemical reaction of the substrate carbon with gas phase Si. This layer was formed to improve the bonding between the coating and the substrate. The CVD layers were not formed on the back side as shown in Fig. 1 and were varied in thickness: 130, 160, and 180 μm. Detailed processing conditions of the CVD process are written elsewhere [10].

In addition to preparing the SiC-coated C/Cs, monolithic SiC was fabricated by the CVD process. The monolithic SiC was at first formed on a graphite substrate

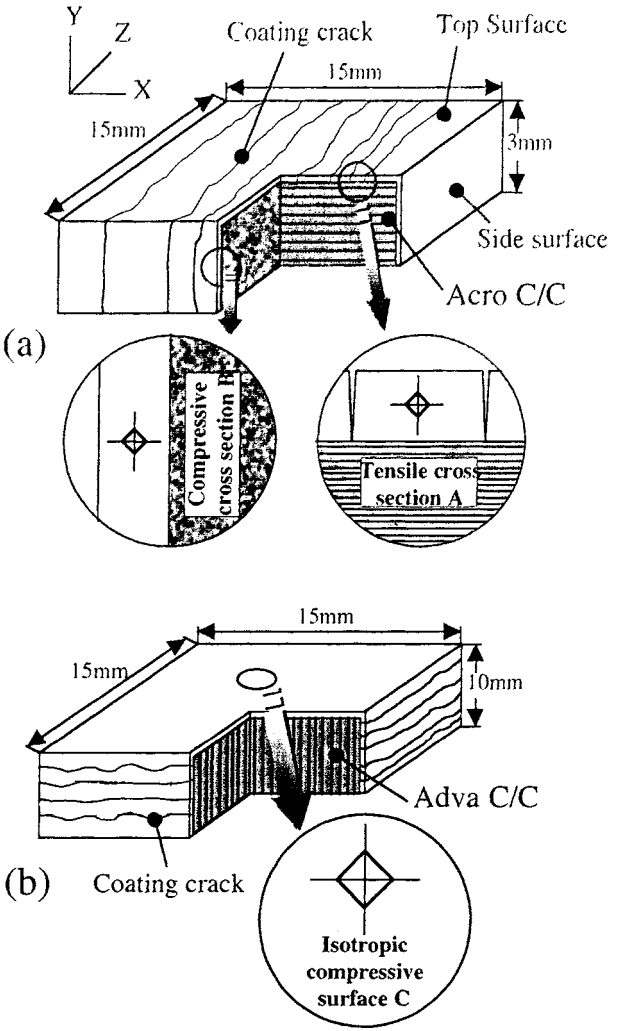

Figure 1. Schematic drawing for specimens of indentation fracture toughness tests. (a) SiC-coated Acro-C/C, (b) SiC-coated Adva-C/C.

(Toyotanso, IG310) under the same processing condition as that used for coating the C/Cs. Then, by grinding and high temperature oxidation, the graphite substrate was removed. The SiC coating on the C/Cs included many cracks due to high thermal stresses, whereas the coating on the graphite did not. Thus, the monolithic SiC was used for the measurements of stress free material.

2.2. Indentation tests

Fracture toughness and thermal stresses were determined by the indentation fracture (IF) method [11–14]. This test was conducted using a micro-hardness tester (Shimadzu: MCTE-501) with a diamond pyramid indenter having an apex angle

of 136°. Before the test, specimen surfaces were polished using diamond paste, gradually reducing particle diameter from 15 μm to 1 μm. After the tests, indentation length and radial median crack length were measured using a laser microscope.

2.2.1. Fracture toughness. The critical stress intensity factor K_c was determined by the indentation fracture (IF) method, following the Japanese industrial standard JIS R 1607. In this standard, equation (1) is used for the determination of K_c:

$$K_c = \alpha(EP)^{1/2}ac^{-3/2}, \tag{1}$$

where α, E, P, a, and c denote constant, Young's modulus, indentation load, half-length of indentation diagonal, and half-length of radial-median crack, respectively. In the JIS, 0.026 is recommended for α. However, in the present study, α was experimentally determined.

The indentation tests were carried out on three types of surfaces, as illustrated in Fig. 1. In the fiber axis direction, the coefficient of thermal expansion, CTE, of the C/Cs are much smaller than that of SiC. Thus, in this direction, high value (~3 GPa) of tensile stress is induced as a result of cooling from coating treatment temperature. This indicates that cracks in the coating occur in the direction perpendicular to the fiber axis. In contrast, in the direction normal to the fiber axis, the CTEs of C/Cs are larger than that of SiC, and compressive stress is induced. Considering that extremely low stress should be induced in the through-the-thickness direction, it is obvious that anisotropic tensile and compressive stress states were induced on cross-sections A and B, respectively, and isotropic compressive stress state on the surface C, as shown in Fig. 1.

2.2.2. Thermal residual stress. In the indentation method, thermal residual stress, the normal stress perpendicular to radial-median crack σ_R, is evaluated by equation (2) [11, 12].

$$K_{res} = K_c - 2\sigma_R(c/\pi)^{1/2}, \tag{2}$$

where K_{res} is an apparent critical stress intensity factor obtained from equation (1) under the existence of residual stress. More precisely, equation (2) neglects effect of interaction of two radial-median cracks emanating to normal directions under an anisotropic stress state. However, in the present study, K_c was obtained from the length of the median crack extending perpendicular to the normal stress we wished to determine.

3. STRESS ANALYSIS

In order to discuss the accuracy of the experimental results, experimentally obtained stresses in the SiC coating were compared with those predicted by the finite element

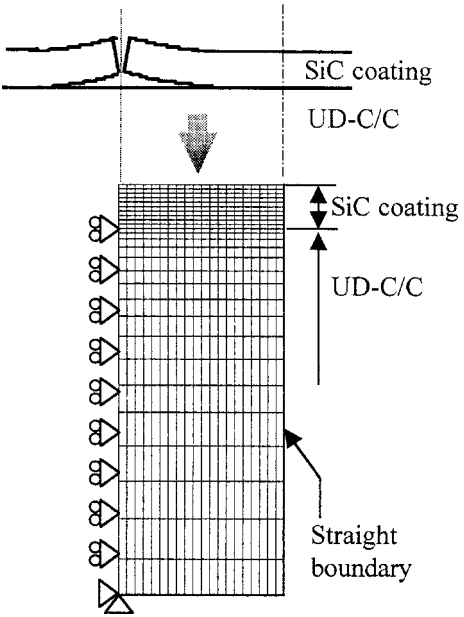

Figure 2. A finite element calculation model for the anisotropic tensile cross-section used to determine stress distribution in SiC coating.

method. An analytical model for cross-section A is shown in Fig. 2, where 8 node-point iso-parametric elements were used under the plane stress assumption. In this cross-section, near periodic through-the-thickness cracks were induced in the coating. Considering symmetry, the half-distance between adjacent coating cracks and actual thickness were included in the model. The whole thickness was used because there was no coating on the back surface. In addition, debonding was observed along the interface between the coating and the C/C, as shown in Fig. 3, and appeared to emanate from the coating cracks. Hence, the model included debonding with an average or maximum length of 35 μm or 90 μm. The calculations simulated thermal stress in the coating when temperature was lowered from coating treatment temperature (1473 K) to room temperature. The material constants used in the calculations are shown in Table 1 [16].

4. RESULTS AND DISCUSSION

4.1. Monolithic SiC

Baseline data were obtained using monolithic SiC with a thickness of 160 μm. The IF tests of monolithic SiC were conducted on the cross-section. The discussion here includes determination of the experimental constant in equation (1), indentation and median-crack length as a function of load, and effective area for the IF tests.

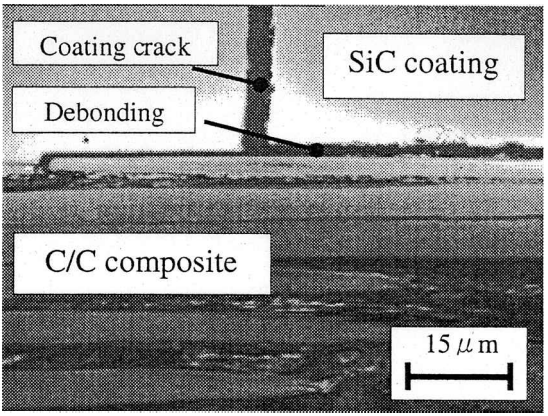

(a)

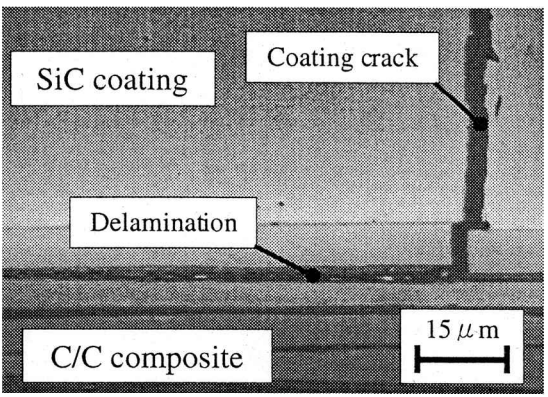

(b)

Figure 3. Cross-sections of SiC-coated C/C composite (Acro-C/C) observed with a laser optical micro-scope. (a) Type A: debonding extending on the coating interface. (b) Type B: delamination running underneath the interface.

4.1.1. Experimental constant. In the IF method, α in equation (1) should be experimentally determined. The IF tests for the determination of α were performed with a changing load along the center line of the monolithic SiC. Figure 4 represents the result, and α was evaluated from the slope [17]. The critical stress intensity factor for CVD-SiC was reported to be 20 J/m^2 ($K_{Ic} = 3.8$ MPa m$^{1/2}$) [18]. The solid line representing this value reasonably fits the experimental results. Thus, α was determined to be 0.031.

4.1.2. Indent and radial-median crack. The indentation length (a) and crack length (c) were measured as a function load (P) as shown in Fig. 5. Theoretically, a and c are proportional to $P^{1/2}$ and $P^{2/3}$, respectively [13, 19]. The solid line and dashed line in the figure are drawn based on this relation. From this figure, it can be confirmed that the present experiments yielded excellent results. Figure 6

Table 1.
Material properties used for calculations of thermal residual stress in the SiC coating

Materials	Young's modulus (GPa)		Shear modulus (GPa) G_{xy}	Poisson's ratio ν_{xy}	Thermal expansion coefficient ($\times 10^{-7}$ 1/K)		Coating thickness (μm)	Test locations
	E_L	E_T			α_L	α_T		
Acro-C/C	200	15	7	0.47	4.6	91	178	Tensile cross-section A
							130	Compressive cross-section B
Adva-C/C	300	25	7	0.47	4.0	90	130	Compressive surface C
SiC (Monolithic)	490		—	0.25	49		178	Cross section

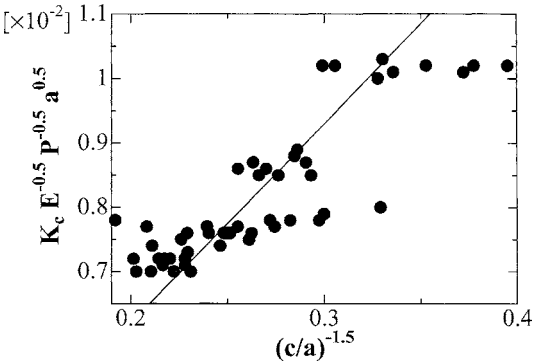

Figure 4. Determination of experimental constant α in equation (1).

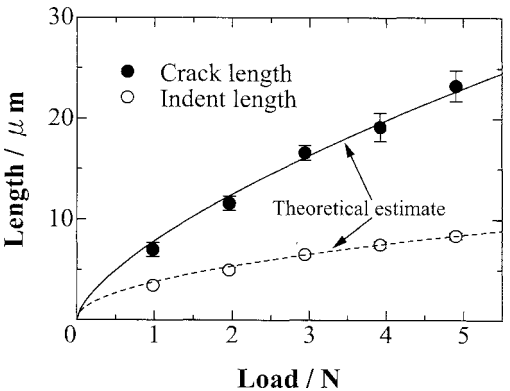

Figure 5. Indent length a and crack length c as a function of applied load in indentation fracture tests.

represents K_{Ic} obtained from the data shown in Fig. 5 and equation (1). This figure demonstrates the constant K_{Ic}. Thus, the IF method is verified to be effective to measure K_{Ic} in a load range of 1 to 5 N. Slight scattering, especially at 1 N, was primarily due to the error in the measurement of c. When the load became smaller than 1 N, crack tips were difficult to identify.

4.1.3. Effective area. When the IF tests were made near the free surfaces, a and c varied with the test location of the thickness direction. In principle, the tests should be performed at locations free from surface effects. To determine this ineffective length, the IF tests were carried out with a changing distance from free surfaces. In these tests, lengths of the cracks depended on the directions. Thus, the four directions of the radial-median cracks were distinguished as A, B, C, and D as shown in Fig. 7b: A and C represent cracks directed normal to the free surface, and B and D that parallel to the free surface. The lengths of A and C, and of B and D under a load of 2 N are plotted in Figs. 7a and b, respectively, as a function of distance from the free surface. Based on these results, the IF tests are regarded as effective when the distance is longer than 40 μm, at which the four cracks extended

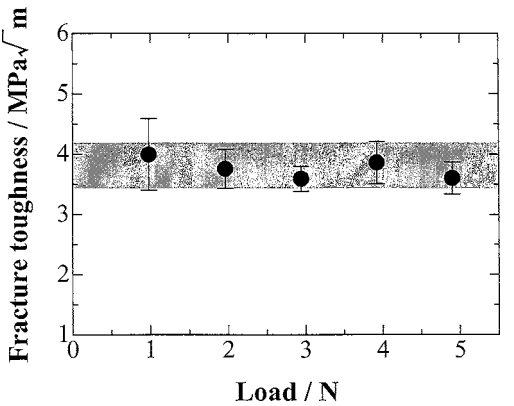

Figure 6. Critical stress intensity factor, K_{Ic}, obtained using equation (1) as a function of applied load in indentation fracture tests.

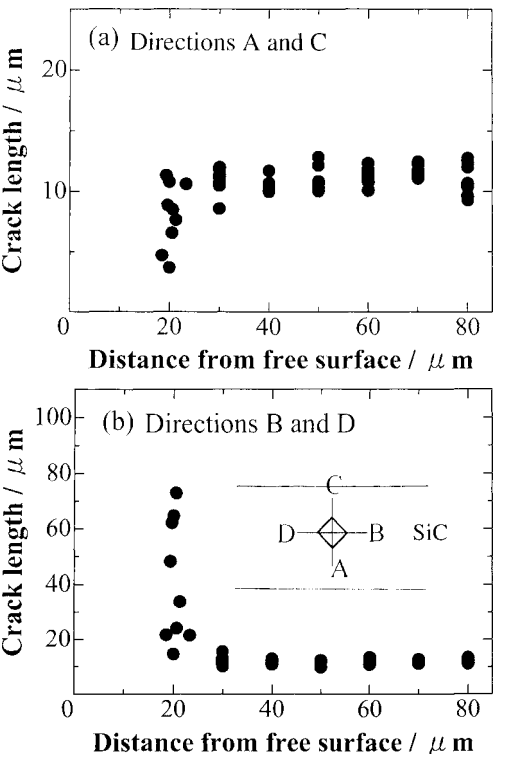

Figure 7. Crack lengths as a function of distance from the free surface propagated in the directions of A and C (a) and B and D (b).

the same length. Then, using crack lengths A and C, apparent K_{Ic} was determined using equation (1), and the results are shown in Fig. 8a and b for loads of 2 N and 4.9 N, respectively. Comparison of Fig. 8 and Fig. 7 reveals that the variation of K_{Ic} derived from differences in the determinations of crack lengths. Based on data like

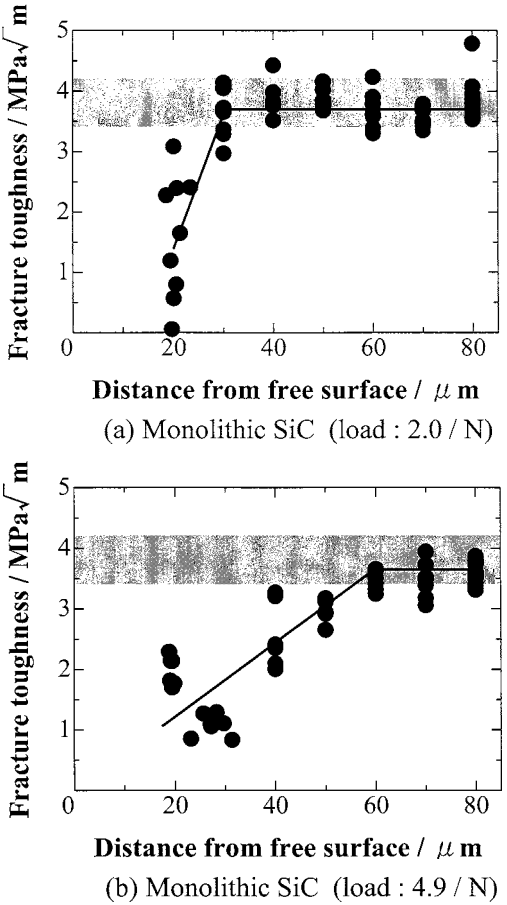

Figure 8. Relation between apparent fracture toughness and distance from the free surface at loads of 2.0 N (a) and 4.9 N (b).

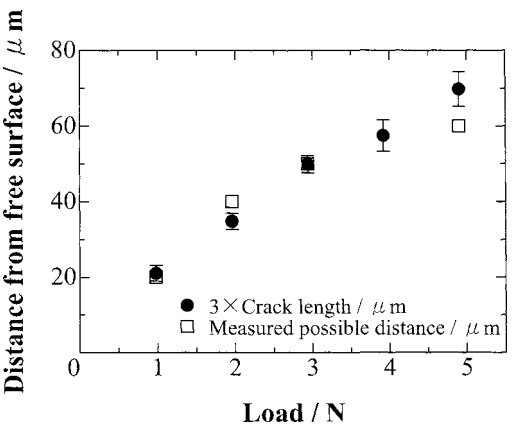

Figure 9. Ineffective distance from the free surface for use of the indentation fracture test as a function of indention load.

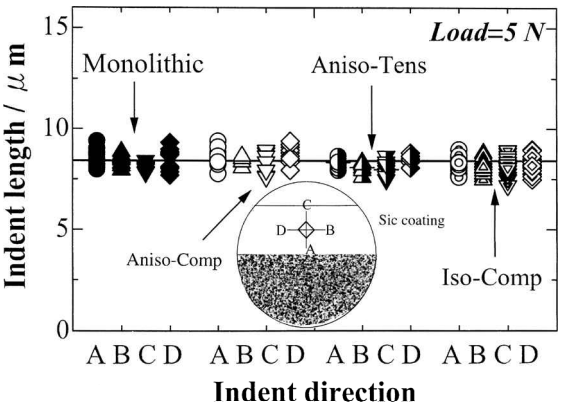

Figure 10. Variation of indent length with directions A, B, C, and D obtained by the IF tests in various stress fields.

those shown in these figures, the distance free from the free surface effect, l, was determined as a function of load, as shown in Fig. 9. In this figure, the length of $3c$ is also plotted, and the distance $3c$ is shown to agree with l. This indicates that the IF tests should be made at a location further than $3c$ from the free surface.

4.2. SiC-coating on C/C

4.2.1. Crack and indent lengths. No thermal stresses are induced in the monolithic SiC, though various residual stress states appears in SiC-coating on C/C, as shown in Fig. 1. However, thermal stress should be extremely low in the thickness direction due to low mechanical restriction from the substrate. Figures 10 and 11 show as and cs for such stress states in the 160 μm SiC coating, where the IF tests were carried out along the center plane of coating under a load of 5 N on the anisotropic tensile cross-section A (Aniso-Tens), anisotropic compressive cross-section B (Aniso-Comp), and isotropic compressive surface C (Iso-Comp). In these figures, A, B, C, and D on the horizontal axis indicate the directions shown in Fig. 10, and the values shown by horizontal solid lines represent the lengths in the monolithic SiC. It can be seen in Fig. 11 that the difference in stress states seriously affected c but not a, as shown in Fig. 10. The crack length becomes larger in the directions of tensile stress, A and C in Aniso-Tens, and becomes shorter in the compressive direction, A and C in Aniso-Comp and all the directions in Iso-Comp. However, the high values in the thickness direction, B and D of Aniso-Comp, are strange, because very low stress is expected in this direction.

4.2.2. Thermal residual stress. Using equation (2) as well as the results in Figs 10 and 11, thermal residual stress σ_{yy} was determined and compared with that by the calculation using FEM. Figure 12 represents the comparison results in the anisotropic compressive cross-section A. The solid and dashed lines in this figure stand for the calculated stresses on the surface and along the interface, respectively,

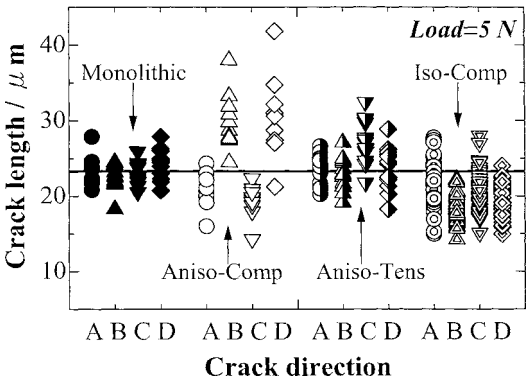

Figure 11. Variation of radial-median cracks with directions A, B, C, and D obtained by the IF tests in various stress fields.

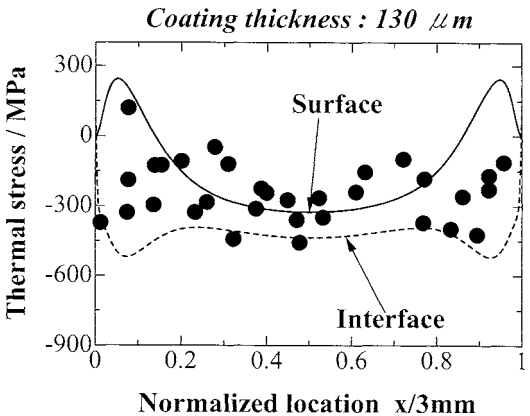

Figure 12. Stress distribution in SiC coating for the anisotropic compressive cross-section B.

and the axis of the abscissa is normalized by the specimen length (L_0) of 3 mm. Figure 12 clearly shows that the experimental and calculated values agree well. This indicates that thermal residual stresses can be measured by the IF method.

Figure 13 shows the thermal residual stresses σ_{yy}s in the isotropic compressive surface C. In this figure, the horizontal axis is normalized by the specimen length (L_0) of 15 mm, and the filled circles represent the calculated stresses on the surface. In this plane, equation (2) is precisely satisfied (isotropic stress state), and the experimental values are scattered around those calculated. Thus, the residual stress σ_{yy} was judged to be very roughly estimated.

In the tensile cross-section B, partial debonding was observed along the coating interface, as shown in Fig. 3a and b. The debonding originated at the coating cracks and extended just on the interface, as in Fig. 3a, or beneath the interface as in b. To evaluate the effect of the debonding, three stress distributions were calculated; i.e. without debonding, and with debonding of the average length, 35 μm, and the maximum length, 90 μm. These three distributions are compared in Fig. 14, where

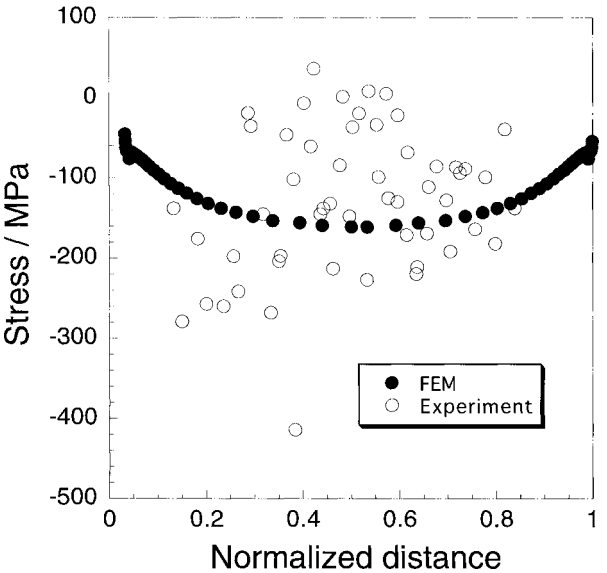

Figure 13. Stress distribution in SiC coating for the isotropic compressive surface C.

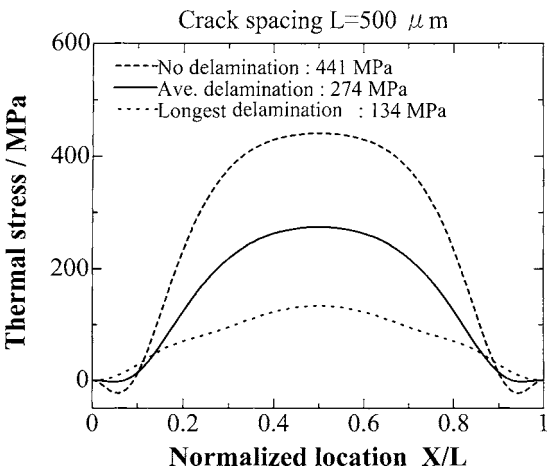

Figure 14. Calculated stress distribution in SiC coating for the anisotropic tensile cross-section A.

the horizontal axis was normalized using the average distance between adjacent coating cracks. As this figure shows, though the maximum thermal stress σ_{yy} without debonding is 440 MPa, it relaxes to 134 MPa when debonding reaches the maximum length. These calculation results were compared with experimental values in Fig. 15, where the solid and dashed lines stand for σ_{yy}s with no debonding and average debonding, respectively. As shown in this figure, experimental values tend to be slightly lower than those calculated, but the difference appears to be within the scattering of experimental results.

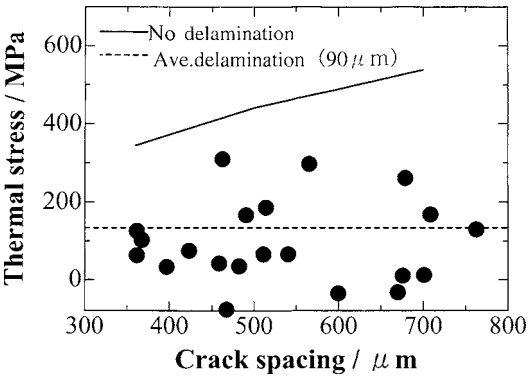

Figure 15. Comparison of calculated and experimentally obtained stress distributions for the anisotropic tensile cross-section A.

As mentioned above, thermal stresses in the SiC coating were reasonably determined by the IF method, except for the stress in the anisotropic compressive cross-section B. In this case, the radial-median cracks in the B and D (thickness) direction became larger than that without thermal stress. However, stress σ_{yy} should essentially vanish in this direction. We do not have a clear explanation for this unexpected result, though we speculated that it is due to the large scattering inherent in SiC [14]. For example, concerning a thicker glass coating, Futakawa *et al.* observed more stable median crack growth and obtained more consistent stress values by the IF method [11].

5. CONCLUSIONS

The indentation fracture method was adopted for SiC coating on C/C composites in order to determine the fracture toughness of the coating and the thermal residual stress induced in the coating. Fracture toughness was determined with an indentation load ranging from 1 to 5 N. In the course of the experiments, it was also shown that a smaller load is preferable for application of a thinner coating. However, determination of crack length becomes more difficult under a smaller load. With regard to thermal stress, the dimension of indentation was shown not to be affected, but crack length was affected. Thus, the indentation method was shown to be effective for rough estimation of thermal stresses, though scattering is large and precise determination is difficult.

Acknowledgement

This research was partly supported by grant-in-aid for basic scientific research (No. 11305047) from the Ministry of Education, Sports, Culture, Science and Technology of Japan.

REFERENCES

1. J. D. Buckley and D. D. Edie, in: *Carbon–Carbon Materials and Composites*, p. 267. NASA Reference Publication 1254 (1992).
2. E. Fitzer, A. Gkogkidis and M. Heine, *High Temperatures — High Pressures* **16**, 363 (1984).
3. E. Fizer, *Carbon* **25**, 163 (1987).
4. B. Dacic and S. Marinkovict, *Carbon* **27**, 549 (1989).
5. E. Yasuda, S. Kimura and Y. Shilsuwa, *Trans. JSCM* **6** (1), 14 (1980).
6. P. L. Walters, F. Rusinko, Jr. and A. G. Austin, *Advances in Catalysis* **11**, 134–217 (1959).
7. G. Savin, in: *Carbon–Carbon Composites*, Chap. 6, pp. 193–219. Chapman and Hall (1993).
8. J. R. Strife and J. E. Sheehan, *Ceram. Bulletin* **67** (2), 369–374 (1988).
9. E. B. Bines, in: *Essentials of Carbon–Carbon Composites*, C. R. Thomas (Ed.), Chap. 8, pp. 204–227. Royal Society of Chemistry (1993).
10. T. Aoki, H. Hatta, Y. Kogo and H. Fukuda, *J. Japan Inst. Metals* **6** (4), 404–412 (1998).
11. M. Futakawa, T. Wakui, R. W. Steinbreck, Y. Tanabe and T. Hara, *Trans. JSME* **A66** (646), 152–158 (2000).
12. Y. Ikuma and A. Virkar, *J. Mater. Sci.* **19**, 2233–2238 (1984).
13. D. B. Marshall and A. G. Evans, *J. Am. Ceram. Soc.* **64C**, 182 (1981).
14. JIS R 1607-1995.
15. A. Okura and T. Chou, in: *Advanced Composites in Emerging Technologies*, pp. 348–353 (1992).
16. H. Hatta, Y. Nakayama, K. Goto, T. Aoki, Y. Kogo and H. Fukuda, *Trans. JSME* **A65** (638), 2073–2079 (1999).
17. G. R. Anstis, P. Chantikul, B. R. Lawn and D. B. Marshall, *J. Am. Ceram. Soc.* **64** (9), 533–538 (1981).
18. T. Hirai, H. Asakura and M. Sasaki, *J. Japan Inst. Metals* **62** (4), 404–412 (1998).
19. B. Lawn, in: *Fracture of Brittle Solids*, 2nd edn, Chap. 8, pp. 249–306. Cambridge University Press (1993).